Size and Shape Dependence of Thermal Spin Transitions in Nanoislands

Pavel F. Bessarab,[1,2] Valery M. Uzdin,[2,3] and Hannes Jónsson[1]

[1]*Science Institute and Faculty of Science, VR-III, University of Iceland, 107 Reykjavík, Iceland*
[2]*Department of Physics, St. Petersburg State University, St. Petersburg 198504, Russia*
[3]*St. Petersburg National Research University of Information Technologies, Mechanics and Optics, St. Petersburg 197101, Russia*

(Received 14 September 2012; revised manuscript received 21 November 2012; published 11 January 2013)

Theoretical calculations of thermal spin transitions in nanoscale clusters on a surface are presented. The mechanisms for magnetization reversal are identified and the activation energy and pre-exponential factor for the rate are evaluated using a recently developed harmonic transition state theory and a Heisenberg-type Hamiltonian. A maximum is found in the pre-exponential factor as a function of cluster size corresponding to a crossover from a uniform rotation mechanism to temporary domain wall formation. As the islands grow, the energy barrier increases up to a limit where the domain wall is fully established. For larger islands, the minimum energy path becomes flat resulting in a significant recrossing correction to the transition state theory estimate of the rate. The parameters of the Hamiltonian are chosen to mimic Fe clusters on a W(110) surface, a system that has previously been studied extensively in the laboratory and the calculated results are found to be in close agreement with the reported measurements.

DOI: 10.1103/PhysRevLett.110.020604 PACS numbers: 75.10.−b, 05.20.Dd

The stability of magnetic states with respect to thermal fluctuations and external perturbations is an important problem in fundamental studies of magnetism and is of critical importance in the design of nanoscale recording devices. The development of scanning tunneling microscopy (STM) and other microscopic scanning probes has made it possible to measure with high resolution and even create and control magnetic structures down to the level of individual spins [1]. The magnetic properties of small clusters can be studied with STM by observation of the Kondo resonance at a particular atom [2] or via measurement of spin polarized current which depends on the relative orientation of magnetic moments in a magnetic tip and the surface atoms [3]. The lifetime of magnetic states at a given temperature can be extracted from such measurements and the rate of transitions thereby determined. Krause *et al.* [4] studied the magnetization reversal process in small Fe clusters on a W(110) surface by spin polarized STM. An Arrhenius dependence on temperature was observed and the results were used to determine the activation energy as well as the pre-exponential factor over a wide range in cluster size and shape. Even for clusters consisting of only a few tens of atoms, the thermally activated magnetization reversal was observed to occur on the time scale of seconds at liquid-nitrogen temperature. In another recent study [5] of antiferromagnetic chains consisting of a few Fe atoms on a Cu_2N surface, the quantum mechanical tunneling as well as thermally activated transitions were measured at 1–10 K. A theoretical estimate of the thermal stability of the magnetization of nanoclusters as a function of size and shape could help in the design of nanoscale devices for data storage with unprecedented capacity.

The long life time of the magnetic states of interest means that transitions between states are rare events on the time scale of spin oscillations and direct simulations of the dynamics would require prohibitively long simulations and large computational effort, analogous to the problem of simulating atomic scale transitions (see, for example, Ref. [6]). The separation of time scales, however, makes it possible to apply statistical approaches. Monte Carlo (MC) simulations with Metropolis sampling do not provide such dynamical information, only thermal averages, but transition state theory (TST) [7], which is based on a statistical estimate of the probability of reaching a transition state, can give an estimate of the rate and also reveal the transition mechanism [6]. A harmonic transition state theory (HTST) for spin transitions has recently been formulated [8] and is used here to analyze magnetization reversal in Fe islands with up to nearly 400 atoms on a W(110) surface, mimicking the experimental system of Krause *et al.* [4]. The results provide information about the transition mechanism as well as quantitative estimates of both the pre-exponential factor and the activation energy for the magnetization reversal. An expression for the HTST approximation to the rate has been derived in Ref. [8]. Here, we only sketch briefly the main ideas of the theory to state clearly the assumptions it rests on.

A general expression for the rate of escape from an initial state is [9]

$$k = \langle \delta[f(\boldsymbol{x})] v_\perp(\boldsymbol{x}) \chi[\boldsymbol{\eta}(t)] \rangle, \tag{1}$$

where $\boldsymbol{x}$ represents all dynamical variables in the system, angular brackets denote the thermal averaging with a Boltzmann distribution, $f(\boldsymbol{x}) = 0$ defines the dividing surface separating the initial state from the rest of configuration space, $v_\perp(\boldsymbol{x}) = \boldsymbol{\nabla} f(\boldsymbol{x}) \cdot \dot{\boldsymbol{x}}$ is the projection of the velocity onto the local normal of the dividing surface. $\chi[\boldsymbol{\eta}(t)]$ is the functional of a full trajectory described by

$\boldsymbol{\eta}(t)$ including coupling to the heat bath and takes the value of unity if a trajectory originating in the initial state goes directly from a point $\boldsymbol{x}$ at the dividing surface to the final state and spends long time there compared with the time it takes to cross the barrier, but is zero otherwise. A convenient choice of the set of variables for a system of N spins is $\boldsymbol{x} \equiv \{\boldsymbol{\theta}, \boldsymbol{\phi}\} \equiv \{\theta_1, \theta_2, ..., \theta_N, \phi_1, \phi_2, ..., \phi_N\}$, where θ_i, ϕ_i are polar and azimuthal angles, respectively, defining the direction of the ith magnetic moment. The magnitude of the magnetic moments is assumed here to be constant and the same for all atoms, i.e., $M_i = M$.

Approximations of the exact expression [Eq. (1)] depend on the choice of $\chi[\boldsymbol{\eta}(t)]$. In the TST approximation, all trajectories pointing away from the initial state at the dividing surface are assumed to be reactive, i.e., the functional $\chi[\boldsymbol{\eta}(t)]$ is approximated by the Heaviside step function, $h[v_\perp(\boldsymbol{x})]$. Thereby, the effect of recrossing the dividing surface is neglected in the TST. Calculations of short time dynamical trajectories can then be carried out starting at the dividing surface to determine the recrossing correction factor [10], κ, and obtain the exact rate, $k = \kappa k^{\mathrm{TST}}$.

A harmonic approximation to the TST estimate is obtained by making a quadratic expansion of the energy at the minimum on the energy surface corresponding to the initial state and at first order saddle points on the energy ridge surrounding the minimum. The harmonic approximation corresponds to choosing a hyperplane of $D-1$ dimensions for a dividing surface, where D is the number of degrees of freedom, $D = 2N$. The hyperplane includes a first order saddle point and has a normal pointing along the unstable mode at the saddle point, the normal mode with a negative eigenvalue. Labeling this mode as q_1, the normal projection of the velocity is $v_\perp(\boldsymbol{\theta}, \boldsymbol{\phi}) = \dot{q}_1$. It can be estimated at each point on the dividing surface using the Landau-Lifshitz-Gilbert equations of motion for magnetic moments (see Ref. [11])

$$\begin{aligned}(1+\alpha^2)\sin\theta_i\dot{\phi}_i &= \frac{\gamma}{M}\left(\frac{\partial E}{\partial\theta_i} - \frac{\alpha}{\sin\theta_i}\frac{\partial E}{\partial\phi_i}\right),\\ (1+\alpha^2)\sin\theta_i\dot{\theta}_i &= -\frac{\gamma}{M}\left(\frac{\partial E}{\partial\phi_i} + \alpha\sin\theta_i\frac{\partial E}{\partial\theta_i}\right),\end{aligned} \tag{2}$$

where γ is a gyromagnetic ratio, α is the damping constant, and E is the energy of the system. These equations become linear with the quadratic approximation to the energy surface. The normal component of the velocity can then be expressed in terms of normal mode coordinates q_i, i.e., displacements along eigenvectors of the Hessian matrix of the energy at the saddle point. The expansion can be written as $v_\perp = \gamma\sum_{i=2}^{D} a_i q_i/M(1+\alpha^2)$, to show explicitly the dependence on α and M. While the velocity through the dividing surface is zero at the saddle point since the gradient of the energy vanishes there, an integration over the hyperplanar dividing surface gives a nonzero reactive flux and the resulting estimate of the rate constant is [8]

$$k^{\mathrm{HTST}} = \frac{\nu}{2\pi}\sqrt{\frac{\det H_m}{\det' H_s}}e^{-(E^s-E^m)/k_BT}, \tag{3}$$

where $\det H_m$ and $\det H_s$ denote the determinants of the Hessian matrices at the minimum and the saddle point, respectively, and ν is defined as

$$\nu = \frac{\gamma}{(1+\alpha^2)M}\prod_{i=1}^{D}\frac{\sin\theta_{s,i}}{\sin\theta_{m,i}}\sqrt{\sum_{i=2}^{D}\frac{a_i^2}{\epsilon_i}},$$

ϵ_i being the eigenvalues of the Hessian at the saddle point and $\boldsymbol{\theta}_s$, $\boldsymbol{\theta}_m$ being polar angles at the saddle point and at the minimum, respectively. The determinants in Eq. (3) are computed as a product of the eigenvalues and the prime means that the negative one, ϵ_1, is omitted. A more general expression valid for the case where the M_i are not constant but depend on orientation can be found in Ref. [8].

Equation (3) predicts an Arrhenius type dependence on the temperature, with an activation energy $E_a = E^s - E^m$ and a temperature independent pre-exponential factor. The HTST rate given by Eq. (3) decreases as the damping constant α becomes larger. This is because the Landau-Lifshitz-Gilbert equations of motion, Eqs. (2), include damping but the effect of recrossing the transition state dividing surface is not taken into account.

Each saddle point corresponds to a specific transition mechanism. For each possible final state, one or more minimum energy paths (MEPs) can be found. Following an MEP involves advancing each degree of freedom of the system in such a way that the energy is minimal with respect to all degrees of freedom perpendicular to the path. The nudged elastic band method [12] is used to find MEPs between a given pair of states. In the calculations presented here, the orientation of the magnetic moment $\boldsymbol{M}_i$ of each atom is included explicitly. This gives a detailed description of the magnetic transitions, including complex mechanisms involving nonuniform rotation of the magnetic moments.

The total energy of the system is approximated here by a classical Heisenberg-type Hamiltonian

$$\begin{aligned}E = &-\sum_n K_n\sum_i(\boldsymbol{M}_i\cdot\boldsymbol{e}_n)^2 - \frac{1}{2}J\sum_{\langle i,j\rangle}\boldsymbol{M}_i\cdot\boldsymbol{M}_j\\ &-\frac{\mu_0}{8\pi}\sum_{i\neq j}\frac{3(\boldsymbol{r}_{ij}\cdot\boldsymbol{M}_i)(\boldsymbol{r}_{ij}\cdot\boldsymbol{M}_j) - r_{ij}^2(\boldsymbol{M}_i\cdot\boldsymbol{M}_j)}{r_{ij}^5}.\end{aligned} \tag{4}$$

The index n in the first sum can take two values, $\parallel$ for easy-axis and $\perp$ for easy-plane anisotropy which results from the interaction with the substrate, J denotes the exchange coupling and $\boldsymbol{r}_{ij}$ the vector between sites i and j. In order to mimic an Fe island on a W(110) substrate, the values of the parameters in Eq. (4) were chosen to be similar to those used in previous MC simulations of thermal properties of Fe islands [4] and a full Fe overlayer on W(110) [13].

A magnetocrystalline easy-axis anisotropy $K_{\|}$ was included along the $[1\bar{1}0]$ direction. The corresponding parameter value was $K_{\|}M^2 = 1.2$ meV which is in between the values that were used in the MC simulations [4,13]. We also included an easy-plane anisotropy $K_{\perp}$ which makes it preferable for magnetic moments to lie in the substrate plane, i.e., in the (110) plane, with $K_{\perp}M^2 = -3.0$ meV. In the MC simulations [4,13], exchange beyond nearest neighbors was included. We used the simplest possible approximation and considered exchange only between nearest neighbors. The nearest neighbor coupling then effectively includes longer range coupling and the effective exchange parameter value is taken to be $JM^2 = 25.6$ meV, twice as big as that for the first nearest neighbors in Refs. [4,13]. Dipole-dipole interaction was included explicitly between each pair of magnetic moments, with $M = 2\mu_B$.

The calculations were carried out for monolayer islands of rectangular shape consisting of 40–364 atoms. The length of the islands along the [001] and $[1\bar{1}0]$ directions, $N_{[001]}$ and $N_{[1\bar{1}0]}$, lies within the range of 9 to 27 atomic rows. The islands have two degenerate states, with spins aligned parallel to the anisotropy axis. The calculations of the MEPs for the magnetization reversal revealed three possible transition mechanisms. Small islands, with $N_{[001]} \leq 13$ and $N_{[1\bar{1}0]} \leq 13$, reverse their magnetization via coherent rotation of all magnetic moments irrespective of the length ratio $N_{[001]}/N_{[1\bar{1}0]}$. However, transitions in bigger islands follow a more complicated path involving nucleation and propagation of domain walls.

Figure 1 shows MEPs of magnetic transitions in three islands with different $N_{[001]}$ but the same $N_{[1\bar{1}0]}$. If an island is longer in the $[1\bar{1}0]$ direction, $N_{[001]} < N_{[1\bar{1}0]}$, then magnetization reversal starts at one of the narrower ends of the island and a domain wall forms perpendicular to the anisotropy axis. The domain wall then moves along the $[1\bar{1}0]$ direction eventually leading to reversal of the magnetization. The energy barrier is determined by the length of the domain wall and thus scales with $N_{[001]}$. However, when $N_{[001]} = N_{[1\bar{1}0]}$, nucleation can equally well start at one of the [001] ends of the cluster, leading to the formation of a domain wall parallel to the anisotropy axis. As $N_{[001]}$ increases, this orientation of a domain wall becomes preferable and the corresponding energy barrier becomes insensitive to changes in $N_{[001]}$.

The dependence of the energy barrier on the size and shape of the islands is illustrated in Fig. 2(a). Three regions, corresponding to three different mechanisms of magnetization reversal, are marked. Region I corresponds to relatively small clusters where magnetization reversal occurs via coherent rotation of all the spins. For the larger clusters, in regions II and III, however, a domain wall forms and propagates during the transition. The domain walls are parallel to the anisotropy axis in region II, while they are perpendicular to the anisotropy axis in region III. For

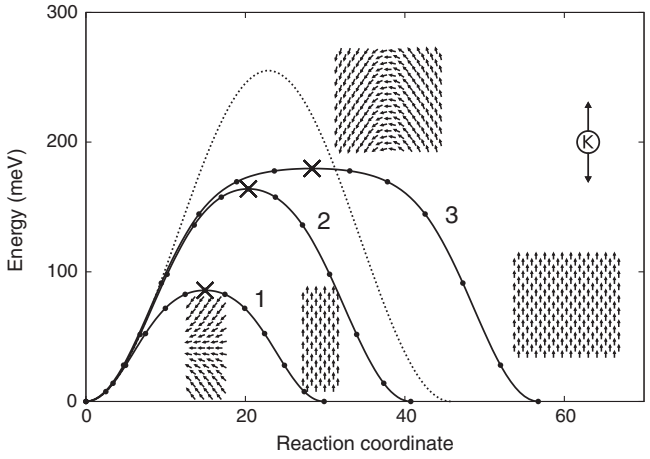

FIG. 1. Minimum energy paths (MEPs) for magnetization reversal in 76, 144, and 212 atom Fe islands. The number of atomic rows in the [001] direction is different for the three islands (curves 1, 2, and 3 correspond to $N_{[001]}$ being equal to 9, 17, and 25, respectively) while the number of atomic rows in the $[1\bar{1}0]$ direction is the same, $N_{[1\bar{1}0]} = 17$. The filled circles show positions of the images in the nudged elastic band calculations. Insets show the orientation of the spins at saddle points and minima for curves 1 and 3 with respect to the anisotropy axis, K. The energy for uniform rotation in the largest island is shown (dotted line) to illustrate how the energy barrier can be lowered by forming a transient domain wall. The reaction coordinate is defined as the displacement along the MEP.

islands with $N_{[001]} = N_{[1\bar{1}0]} \geq 15$ both orientations of the domain wall are possible and give similar energy barriers.

All but one of the islands reported in the experimental study of Krause *et al.* [4] correspond to region II. The calculated values of the energy barrier for clusters within this region are shown in Fig. 2(b) as a function of $N_{[1\bar{1}0]}$ as well as the experimental estimates. The agreement between the calculated and the measured values is good and a clear linear dependence on the domain wall length, i.e., $N_{[1\bar{1}0]}$, is seen in both cases. However, the calculated barrier is systematically too small for the smaller islands. This might be due to a rim effect where the anisotropy for rim atoms is larger [4].

The pre-exponential factor is also strongly dependent on the size and shape of the islands. Figure 3(a) shows the HTST estimate evaluated from Eq. (3) as a function of $N_{[001]}$ and $N_{[1\bar{1}0]}$. The figure shows that the pre-exponential factor is largest for islands with the same number of atomic rows along both sides. Furthermore, a small maximum occurs for islands with $N_{[001]} = N_{[1\bar{1}0]} \approx 15$ [see also Fig. 3(b)]. Both of these features are in remarkably good agreement with the experimental data, which however is available mainly for region II. The analogous contour plot in Ref. [4] shows a similar ridge formation for $N_{[001]} = N_{[1\bar{1}0]}$ with a maximum in a similar position as in the calculations. The four experimental data points for

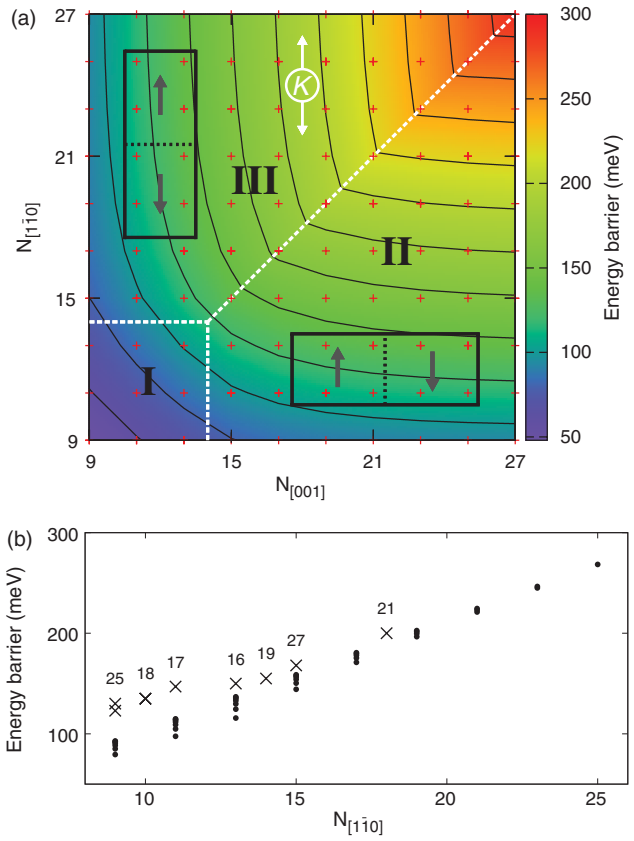

FIG. 2 (color). (a) Contour plot of the calculated energy barrier as a function of the number of atomic rows along the [001] and $[1\bar{1}0]$ directions. In region I, the transition mechanism involves uniform rotation. In regions II and III the transition involves formation of a transient domain wall along the $[1\bar{1}0]$ direction or the [001] direction, as illustrated in the insets. The easy-axis anisotropy is along the $[1\bar{1}0]$ direction. Red crosses indicate the calculated data points; linear interpolation, first along the diagonal and then along horizontal and vertical lines, was used to generate the figure. (b) Calculated (filled circle) and measured (crosses) (from Ref. [4], with $N_{[001]}$ shown above data points) energy barrier as a function of the number of atomic rows in the $[1\bar{1}0]$ direction. All calculated points for all islands in region II are shown.

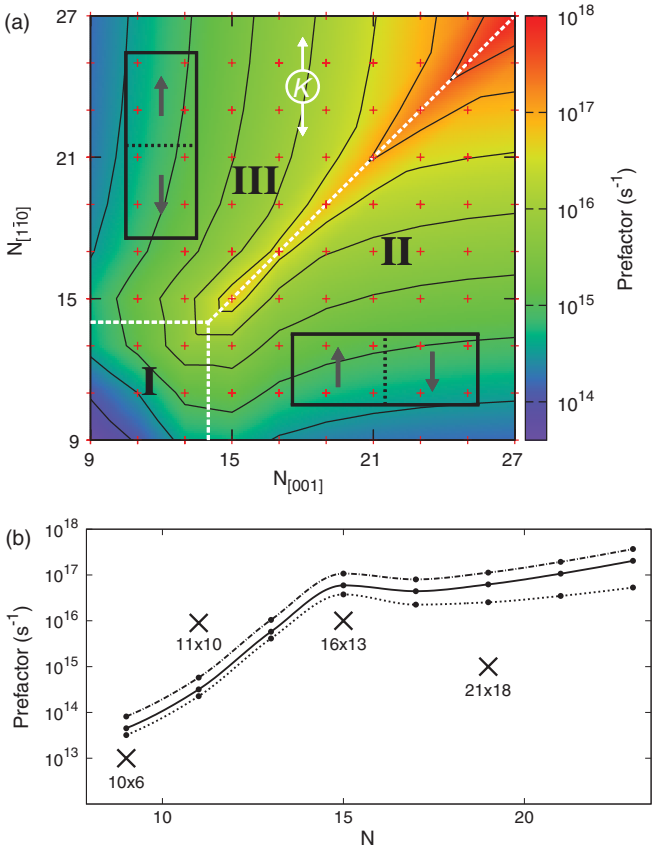

FIG. 3 (color). (a) Contour plot of the calculated HTST pre-exponential factor as a function of the number of atomic rows along the [001] and $[1\bar{1}0]$ directions. Regions I, II, and III are marked according to the transition mechanism as in Fig. 2(a). A maximum along the diagonal is formed for island with ~100 atoms, similar to what has been observed experimentally [4]. Red crosses indicate the calculated data points; linear interpolation, first along the diagonal and then along horizontal and vertical lines, was used to generate the figure. (b) Calculated pre-exponential factor for transitions in islands with the same number of atomic rows on both sides as a function of the number of atomic rows on a side. The data points (filled circle) connected by a solid line show calculated results using the HTST. Experimental estimates for islands that are close to the line $N_{[001]} = N_{[1\bar{1}0]}$ are marked with crosses (from Ref. [4], with the estimated dimension shown below the crosses). The dotted line includes approximate corrections for recrossings of the transition state assuming Langevin dynamics (see Eq. (1) in Ref. [17]) and the dash-and-dot line corresponds to zero damping.

islands that are closest to having the same number of atomic rows on both sides are shown in Fig. 3(b).

The calculated results have a simple interpretation. For islands with $N_{[001]} = N_{[1\bar{1}0]}$ there is a crossover between transition mechanisms involving domain walls with the two different orientations. This increases the entropy of the transition state which in turn leads to a larger value of the pre-exponential factor. The maximum obtained for clusters with $N_{[001]} = N_{[1\bar{1}0]} \approx 15$ atomic rows corresponds to a point where three possible transition mechanisms become equally likely, resulting in an even larger entropy of the transition state.

In Ref. [4], the increase of the pre-exponential factor with increasing $N_{[1\bar{1}0]}$ while $N_{[001]}$ is kept constant was ascribed to multiple nucleation sites at the [001] end of an island. Each nucleation center would add a new pathway for a transition leading to a larger pre-exponential factor. However, the calculations do not show evidence of this. There, the domain wall formation always involves all spins along the side of an island so the clusters studied here are small compared to the critical nucleus.

Although the application of the HTST to thermal magnetic reversal in the islands described above gives quite

satisfactory agreement with the experimental data and provides an interpretation of the observed trends, the flatness of the energy profile along the minimum energy path for the larger islands makes recrossings of the transition state dividing surface more likely, thereby causing the TST expression, Eq. (3), to give an overestimate. An estimate of the effect of such recrossings has been developed assuming a Langevin description of the dynamics [14–16]. This approach was extended recently in the context of micromagnetic modeling [17]. Figure 3(b) shows the estimated reduction in the pre-exponential factor using this approach when the damping constant is chosen to be $\alpha = 0.9$, the value giving a maximal recrossing effect within this level of approximation. A more accurate estimate of the recrossing correction can be obtained from dynamical trajectories started from points on the transition state dividing surface [10]. A recent example of such an approach for atomic systems is given in Ref. [18]. A simple Langevin description of the recrossing dynamics in atomic scale systems has proven to be too crude [19] and may be giving an underestimate of the recrossing correction in the present case. It remains to be seen from direct calculations of recrossing trajectories to what extent a Langevin description of the dynamics is adequate. The HTST formulation of the rate theory makes it possible to introduce various levels of accuracy of the recrossing correction.

This work was supported by The Icelandic Research Fund, The University of Iceland Scholarship Fund, RFBR Grant No. 12-02-31716, and DFG-RFBR Cooperative Grant: DFG No. ZA 161/20-1; RFBR No. 11-02-91337. We gratefully acknowledge helpful discussions with Dr. S. Krause and Dr. G. Herzog.

[1] R. Wiesendanger, Rev. Mod. Phys. **81**, 1495 (2009).
[2] V. Madhavan, W. Chen, T. Jamnella, M. F. Crommie, and N. S. Wingreen, Science **280**, 567 (1998).
[3] D. Serrate, P. Ferriani, Y. Yoshida, S.-W. Hla, M. Menzel, K. von Bergmann, S. Heinze, A. Kubetzka, and R. Wiesendanger, Nat. Nanotechnol. **5**, 350 (2010).
[4] S. Krause, G. Herzog, T. Stapelfeldt, L. Berbil-Bautista, M. Bode, E. Y. Vedmedenko, and R. Wiesendanger, Phys. Rev. Lett. **103**, 127202 (2009).
[5] S. Loth, S. Baumann, C. P. Lutz, D. M. Eigler, and A. J. Heinrich, Science **335**, 196 (2012).
[6] H. Jónsson, Proc. Natl. Acad. Sci. U.S.A. **108**, 944 (2011).
[7] E. Wigner, Trans. Faraday Soc. **34**, 29 (1938).
[8] P. F. Bessarab, V. M. Uzdin, and H. Jónsson, Phys. Rev. B **85**, 184409 (2012).
[9] W. H. Miller, Acc. Chem. Res. **9**, 306 (1976).
[10] J. C. Keck, Adv. Chem. Phys. **13**, 85 (1967).
[11] H. B. Braun, Phys. Rev. B **50**, 16 501 (1994).
[12] G. Henkelman, B. Uberuaga, and H. Jónsson, J. Chem. Phys. **113**, 9901 (2000); **113**, 9978 (2000).
[13] A. Bergman, A. Taroni, L. Bergqvist, J. Hellsvik, B. Hjörvarsson, and O. Eriksson, Phys. Rev. B **81**, 144416 (2010).
[14] H. A. Kramers, Physica (Amsterdam) **7**, 284 (1940).
[15] J. S. Langer, Ann. Phys. (N.Y.) **54**, 258 (1969).
[16] W. T. Coffey, D. A. Garanin, and D. J. McCarthy, Adv. Chem. Phys. **117**, 483 (2001).
[17] G. Fiedler, J. Fidler, J. Lee, T. Schrefl, R. L. Stamps, H. B. Braun, and D. Suess, J. Appl. Phys. **111**, 093917 (2012).
[18] C.-Y. Lu, D. E. Makarov, and G. Henkelman, J. Chem. Phys. **133**, 201101 (2010).
[19] R. F. Grote and J. T. Hynes, J. Chem. Phys. **73**, 2715 (1980).